TECHNICAL MEMORANDUM

396

Retrieving N_2O from nadir viewing infrared spectrometers

A.M. Lubrano[1], G. Masiello[2], M. Matricardi and C. Serio[1]

Research Department

[1]Istituto Nazionale per la Fisica della Materia, Unità di Napoli, Gruppo Collegato di Potenza, C.da Macchia Romana, 85100 Potenza, Italy

[2]Istituto di Metodologie Avanzate di Analisi Ambientale del CNR Tito Scalo, Pz, Italy

Submitted to Tellus B

January 2003

European Centre for Medium-Range Weather Forecasts
Europäisches Zentrum für mittelfristige Wettervorhersage
Centre européen pour les prévisions météorologiques à moyen terme

For additional copies please contact

The Library
ECMWF
Shinfield Park
Reading
RG2 9AX
library@ecmwf.int

Series: ECMWF Technical Memoranda

A full list of ECMWF Publications can be found on our web site under:
http://www.ecmwf.int/publications/

Abstract

The paper describes and demonstrates a methodology for the physical retrieval of nitrous oxide that uses the spectral radiance measured by the next generation of high-resolution satellite-borne infrared sensors. The performance of the retrieval scheme has been assessed on the basis of numerical exercises. Examples of retrievals based on IMG spectra measured over the sea surface are given to demonstrate the ability of the scheme to obtain accurate N_2O concentration values.

1 Introduction

Nitrous oxide (N_2O) is an important greenhouse gas with an atmospheric lifetime of 120 years. It is mostly produced by microbial processes in soils and increases with intensified land use, especially as a result of fertilization. The N_2O level in the lower troposphere is monitored by the Climate Monitoring and Diagnostic Laboratory (CMDL) of the National Oceanic and Atmospheric Administration (NOAA) through measurements made at a world-wide distributed network of stations (for further information see http://www.cmdl.noaa.gov). These measurements set the present value of N_2O concentration at $\approx$ 0.32 ppmv with a 0.3%/year increase.

Nitrous oxide plays an important role in atmospheric chemistry: the dissociation of N_2O by excited oxygen atoms is the major source of nitrogen oxides (NO_x=NO, NO_2, which are important in determining the distribution of both tropospheric and stratospheric ozone (Liou, 1992).

The long lifetime of N_2O suggests that its spatial variability should be extremely low. However, as a likely result of intensified land use and anthropogenic activities, in situ measurements (e.g., NOAA web site, see also WMO (2001)) show that the inter annual variability of N_2O concentration can reach peaks of $\pm$ 5-7% around the annual mean. It is not clear at the moment whether or not this temporal variability is paralleled by an equivalent spatial variability.

Given the current and future availability of satellite observations at high spatial resolution, in this paper we have examined the feasibility of N_2O retrieval from space. A strategy for the physical retrieval of N_2O profiles is described which applies to the current and future generation of high-resolution infrared sounders as the Atmospheric Infrared Sounder (AIRS) on the AQUA satellite (lauched in 2002), the Geosynchronous Imaging Fourier Spectrometer (GIFTS) on the EO-3 platform (to be lauched in 2005), the Infrared Atmospheric Sounding Interferometer (IASI) on the METOP platform (to be lauched in 2005) and the Cross Track Infrared Sounder (CrIS) on the NPP (launch date 2006) and NPOESS (to be lauched in 2008) satellites. All these spectrometers are characterized by a broad band spectral coverage ($\approx$ 3.7 to 15.5 μm) and a spectral sampling rate in the range 0.25 to 1 cm^{-1}.

Two inversion schemes have been developed and tested. The first one is based on a non-parametric estimation approach where no special assumptions other than the ones contained in the first guess is made about the shape of the N_2O profile. In the second scheme, however, the observed profile is parameterised in terms of the reference vertical concentration and therefore results in a lower number of degrees of freedom in the final solution. Since N_2O is an uniformly mixed gas, it will be shown that the parametric estimation approach performs as good as the non-parametric one.

The retrieval of the concentration of an atmospheric gas from infrared radiance requires an a-priori knowledge of the temperature profile. Because of the wide spectral range covered by the new generation of infrared sensors, the temperature profile can be obtained from the inversion of the spectral radiance in suitable spectral ranges and then used to perform the retrieval of the concentration of the gas specie by using the radiance measured in a different (and not-overlapping) spectral region. In this paper we have used the following approach. The CO_2 absorption band at 14-μm is used with part of the atmospheric window at 11-μm (the 800 to 830 cm^{-1}

and 1100 to 1200 cm^{-1} spectral regions rich of weak water vapor lines) to perform the simultaneous retrieval of the temperature and water vapour profiles. This information is then used in a sequential retrieval approach to retrieve the N_2O profile using a portion of its ν_3 fundamental band at 4.5 μm.

To demonstrate the ability of the method to retrieve N_2O concentration profiles from space, a set of IMG spectra have been used. The Interferometric Monitoring of Greenhouse Gases (IMG) (Kobayashi et al, 1999) has flown on board the Japanese Advanced Earth Observing Satellite (ADEOS) from October 1996 to June 1997. The instrument is a Fourier Transform Spectrometer that observes Earth's emission spectrum at nadir in three spectral bands from 3.3 to 16 μm with a nominal spectral sampling of 0.05 cm^{-1}.

The paper is organized as follows. Section 2 describes the choice of the spectral range used for the retrieval of N_2O, the strategy for the inversion and summarizes the details relevant to the radiative transfer calculations. Section 3 describes the physical retrieval approach and the assessment of its performance. Section 4 shows examples of retrievals based on IMG spectra. Conclusion are drawn in section 5.

2 The inversion strategy and background

To perform the retrieval of N_2O profiles we need

1. a radiative transfer model to simulate the observed radiance spectrum,
2. a suitable spectral range that is mostly sensitive to N_2O and where the contamination from other absorbing gases is negligible,
3. information about temperature and water vapor vertical distribution.

These three basic aspects will be here discussed.

2.1 Radiative transfer calculations

All the radiative transfer calculations presented in this paper have been performed using the σ-IASI code ((Amato et al, 2002)), a fast line-by-line model that, in addition to spectral radiance, can compute analytical Jacobians for the major geophysical parameters (e.g. temperature, water vapor, ozone, carbon dioxide, nitrous oxide). Although the code has been developed mostly for IASI, it is well suited for nadir viewing satellite and airplane infrared sensors with a sampling rate in the range 0.1-2 cm^{-1}. The code computes monochromatic radiances from look-up tables of monochromatic layer optical depth generated using the line-by-line model LBLRTM (Clough et al, 1992). Following the LBLRTM strategy, for each individual species, the monochromatic layer optical depth is generated and stored in the appropriate look-up table at a sampling rate, $\Delta\sigma$, equal to 0.25 times the width of the narrowest gas absorption line, which gives for the highest-altitude layer $\Delta\sigma = 0.000169$ cm^{-1}. The code σ-IASI borrows from LBLRTM the CO_2 line mixing scheme. Cross sections of heavy molecules such as chlorofluorocarbons are not parameterized in terms of look-up tables, since absorption can be quickly computed separately. The code σ-IASI accounts for the presence of CFC species, namely CCl3F (CFC-11) and CCl2F2 (CFC-12). Water vapor continuum absorption is computed separately; we use the CKD standard (Clough et al, 1989), version 2.4. The atmospheric layering embedded in σ-IASI consists in a pressure layer grid of $N_l = 44$ grid points defined in Tab. 1. All the required spectroscopic parameters have been extracted from the database HITRAN 96 (Rothman et al, 1998). Further details about σ-IASI may be found in Amato et al (2002).

To simulate the observations, the σ-IASI monochromatic radiance is convolved with a pure cardinal sine function, whose parameters are set up to correspond to the instrumental line shape of an ideal interferometer spectrometer of maximum optical delay of 2 cm, and, finally, apodized with a Gaussian function of 0.25 cm^{-1} half-width half-height. For consistency IMG spectra have been apodized with the same function as that used for the synthetic spectral radiance. The sampling rate of the final spectra (simulated and observed) is $\Delta\sigma = 0.25$ cm^{-1}. This choice matches the sampling rate of most of the modern nadir viewing sensors which are planned to fly in this decade.

The reason for the Gaussian apodization is twofold. First the Gaussian apodization is consistent with what for now has been prescribed for the IASI level 1C data, so that our calculations yield IASI-like spectra.

Second, this study is mostly based on IMG spectra whose nominal sampling rate is 0.05 cm^{-1}. However, one has to bear in mind that the spectral response function of IMG is not well characterized: it differs from the theoretical cardinal sine function mostly because of self-apodisation. The Gaussian apodization (Lubrano et al, 2000) limits the problems of self-apodization and allows us to compare observations and calculations on the basis of a common instrumental line shape. The rationale of the method is that under apodization with a known mathematical function, $w(\sigma)$, the unknown spectral response function, $\tilde{I}(\sigma)$, transforms to:

$$I(\sigma) = \int_{-\infty}^{+\infty} \tilde{I}(\sigma_o) w(\sigma - \sigma_o) d\sigma_o \tag{1}$$

and we have $I(\sigma) \approx w(\sigma)$ provided that w is much wider than the unknown $\tilde{I}(\sigma)$. To this end, we have used a re-sampling rate $\Delta\sigma = 0.25$ cm^{-1}, which is 5 times larger than the IMG nominal sampling rate.

To model the observational noise, the covariance matrix of observations undergoes the same kind of transformations (e.g. Amato et al (1998)) and therefore is properly scaled to the new sampling rate resolution. In this analysis the covariance matrix has been built up by the IMG radiometric noise figures obtained at the proto flight level. Figure 4 shows the IMG radiometric noise for the range 2190-2215 cm^{-1} before and after the re-sampling operation.

In this study all the radiance spectra have been computed for a nadir view and assuming a sea surface. To compute the emissivity of a sea surface, the Masuda model has been used (Masuda et al, 1988).

2.2 Choice of the N_2O spectral range

Nitrous oxide has three main vibrational bands in the infrared centred at 1284.91 cm^{-1} (ν_1), 588.77 cm^{-1} (ν_2), and 2223.76 cm^{-1} (ν_3), respectively. The ν_2 fundamental band is outside the range of current and planned infrared sensors and therefore is not considered here. The ν_1 band overlaps the methane ν_4 band centred at 1310.76 cm^{-1} and the H_2O main vibrational band centred at 1594.75 cm^{-1}. Given the sampling rate (between 0.25 and 2 cm^{-1}) of the sensors considered here, the use of the N_2O ν_1 band has to be dismissed since the contribution of H_2O and CH_4 to the observed spectral radiance makes too difficult to disentangle the concentration of N_2O from that of the other two conflicting gases.

The ν_3 band overlaps in part the ν_3 band of CO_2. However, CO_2 is much less variable than H_2O, methane and N_2O itself. Unless we consider polluted areas, CO_2 natural inter-annual variability is less than 2% to be compared with an observed peak value of 5-7% (e.g. WMO (2001))for N_2O .

Figure 1a shows the plot of the difference

$$\Delta_1 = S_{\mathrm{ref}}(\sigma) - S+(\sigma) \tag{2}$$

where $S_{\mathrm{ref}}(\sigma)$ is the spectral radiance at a wave number σ computed for a reference tropical air mass (e.g. Anderson et al (1986)) and $S+(\sigma)$ is the computed spectral radiance for the same atmospheric profile with the

N_2O concentration increased by +5% at each layer. The plot of the difference clearly shows the N_2O absorption band which extends approximately from 2150 to 2270 cm^{-1}.

Figure 1b shows the difference (Δ_2 in figure 1b) between $S_{ref}(\sigma)$ and $S+(\sigma)$ where $S+(\sigma)$ has now been obtained by simultaneously increasing the CO_2 and N_2O profiles by 2% and 5% respectively. The difference $\Delta_3 = \Delta_1 - \Delta_2$ is shown in Fig. 1c. It can be seen that the region 2170-2215 cm^{-1} is not affected by CO_2 absorption (at least at the sampling rate of 0.25 cm^{-1}). The region 2170-2190 cm^{-1} has still some important water vapour spectral features. In order to minimize the possible interference from water vapour, we selected the spectral region used for the retrieval of N_2O to be in the range 2190–2215 cm^{-1}.

2.3 Temperature and water vapor information

Atmospheric gas retrieval in the infrared depends critically on the vertical distribution of temperature. In addition, absorption from water vapor can also be important because of its potential interfering effects. The strategy we have devised is to adopt a sequential retrieval scheme in which skin temperature, temperature and water vapor are simultaneously retrieved at the first step. The spectral ranges used for the retrieval are

1. 645 to 830 cm^{-1}
2. 1100 to 1200 cm^{-1}

The first spectral interval overlaps the longwave absorption band of CO_2 and is used here mostly for temperature. The range 1100 to 1200 cm^{-1} provides information about water vapor in the lower and middle atmosphere.

The inversion algorithm used for temperature and water vapor is discussed by Lubrano et al (2000). As an example, the algorithm has been used to derive the temperature and water vapour profiles shown in Fig.s 2 and 3 from a mid-latitude winter IMG spectrum and from a tropical IMG spectrum respectively. Aslo shown in the figures is the temperature profile provided by the analysis from the European Centre for Medium Range Weather Forecasts (ECMWF). Note that above 10hPa the ECMWF temperature profile is supplemented with the temperature profile retrieved by the national Environmental Satellite Data and Information Service (NESDIS). This is because at the time the IMG spectra were recorded, the top of the vertical pressure grid used in the ECMWF global atmospheric model was placed at 10 hPa. In Fig.3 the temperature profile is plotted using a logarithmic scale to ease the comparison in the upper atmosphere. The Mid-latitude Winter type IMG spectrum was recorded over the Mediterranean sea on 3 Apr 1997, at GMT 21:36:00.88, whereas the tropical spectrum was recorded over the Indian Ocean on 6 May 1977, GMT: 07:18:24.93. The two IMG spectra were resampled at the sampling rate of 0.25 cm^{-1} before inversion for temperature and water vapor. Both spectra will be used again in section 4 to exemplify the application of the N_2O retrieval methodology to real observations.

3 N_2O Retrieval Methodology and Analyses

3.1 Non-parametric approach

Nitrous oxide is retrieved at the N_l=44 pressure-grid points defined in Tab. 1, according to the regularized inverse equation (e.g. see Carfora et al (1998) and references therein):

$$\delta\hat{\mathbf{q}} = (\mathbf{K}'\mathbf{S}^{-1}\mathbf{K} + \gamma\mathbf{B}^{-1})^{-1}\mathbf{K}'\mathbf{S}^{-1}\delta\mathbf{r} \tag{3}$$

whit the prime indicating *tanspose* and where

1. $\delta\mathbf{r} = \mathbf{r} - \mathbf{r}_o$; with $\mathbf{r}$ the observed radiance vector and $\mathbf{r}_o$ the *reference* or first guess radiance vector
2. $\delta\hat{\mathbf{q}} = \hat{\mathbf{q}} - \mathbf{q}_o$; with $\mathbf{q}$ the estimated N_2O concentration vector and $\mathbf{q}_o$ the *reference* or first guess N_2O concentration vector
3. $\mathbf{S}$ is the covariance matrix of the observations
4. $\mathbf{K}$ is the N_2O Jacobian or derivative matrix computed at $\mathbf{q}_o$.
5. $\mathbf{B}$ is a smoothing operator
6. γ is the regularization parameter

The smoothing operator $\mathbf{B}$ is here defined to be the exponential covariance function:

$$B(i,j) = v(i)v(j)\exp\left(-\frac{\mid p_i - p_j \mid}{\Delta p}\right) \tag{4}$$

where p_i the pressure value at the i-th point of the pressure layer grid (see Tab. 1). In this study we have chosen $\Delta p = 1.3$ hPa which gives a quasi-diagonal B-matrix whose diagonal elements are $v(1),\ldots,v(N_l)$=$\mathbf{v} = 0.2\mathbf{q}_o$ which means that the expected variability of the N_2O profile is within 20% of its reference value $\mathbf{q}_o$. This choice is empirical and is not based on real observations that for N_2O are rare (at least as far as its vertical distribution is concerned). The nature of this constraint is rather mathematical than statistical. For this reason we include also an additional smoothing parameter, γ, in order to optimally tune the smoothness of the final solution. The optimal value of γ is chosen by using the so called L-curve criterion (Hansen, 1992).

Finally, the covariance matrix of the observations $\mathbf{S}$ is defined based on the radiometric noise figure for IMG (see, Fig. 2). Once the covariance matrix $\mathbf{S}$ is specified, the covariance matrix $\mathbf{C}$ used in the inversion process is derived from Eq. (3) (see, e.g. Kendall and Stuart (1979)):

$$\mathbf{C} = (\mathbf{J}'\mathbf{J} + \gamma_{opt}\mathbf{B}^{-1})^{-1}\mathbf{J}'\mathbf{J}(\mathbf{J}'\mathbf{J} + \gamma_{opt}\mathbf{B}^{-1})^{-1} \tag{5}$$

where $\mathbf{J}$ is the normalized jacobian: $\mathbf{J} = \mathbf{S}^{-\frac{1}{2}}\mathbf{K}$ and γ_{opt} is the optimal value of the regularization parameter.

3.1.1 Assessment of the profiling accuracy

The analysis presented here use the TIGR data base (Chedin et al, 1985) in the form made available to the IASI Sounding Science Working Group (ISSWG). This database consists of a set of 2311 radiosonde profiles for temperature and water vapor supplemented by a set of 383 ozone profiles from the NESDIS.

For the assessment of the performance of the retrieval scheme, a subset of 100 profiles were selected at random for each air-mass type. We use the usual climatological classification (Anderson et al, 1986) for the air mass: Tropical, Mid-latitude Summer, Mid-latitude Winter, High-latitude Summer and High-latitude Winter. The total number of selected profiles was therefore 500. Profiles for the minor and trace gases were obtained from the Air Force Geophysical Laboratory (AFGL) compilation (Anderson et al, 1986).

For each of the 500 selected profiles, synthetic IASI-like radiances were computed using the σ-IASI code. Three basic sets of radiances were generated: the first was obtained by using a reference climatological profile for N_2O whereas the other two were obtained by perturbing the reference N_2O profile by $\pm$ 5%.

The N_2O concentration profile after perturbation $q(p)$ (p here is the pressure) can be written as a function of the reference profile $q_o(p)$ using the following equation:

$$q(p) = q_o(p)\,(1 + \pi(p)) \tag{6}$$

where the scaling factor $\pi(p)$ can be written as a function of a *magnitude* f_o and a *scale height* h_p

$$\pi(p) = f_o \exp\left(\frac{p - p_o}{h_p}\right) \tag{7}$$

here p_o denotes the pressure at ground level. Equation 6 can be used to define the perturbed N_2O profile in the most general way. A systematic perturbation can for instance be obtained by setting $h_p = \infty$. By properly assigning the scale height we can simulate perturbations that occur at low altitudes or in localised regions such as those expected to be generated in the lower atmosphere because of antrophogenic activities. However, later in this and the next section we will show that we are only able to retrieve a perturbed profile that has been assigned a scale height that tends to infinity: perturbations localised at low-altitudes cannot be resolved in the infrared unless we use spectra measured over surfaces with a very low emissivity.

It should be stressed here that given the long lifetime of N_2O we expect the gas to be uniformly mixed so that we can reasonably assume that the shape of the profile is known: we are looking for the occurrence of a shift with respect to a reference value.

Keeping this in mind, the perturbed data set was used to generate the observations (addition of observational noise according to the covariance matrix specified in the previous section). Using the reference set as the first guess, the perturbed N_2O profiles were retrieved according to the sequential methodology outlined above, that is:

- the radiance in the spectral intervals 645 to 830 cm^{-1} and 1100 - 1200 cm^{-1} is used to retrieve the temperature and water vapour profiles.
- the N_2O profile is retrieved using 1) - the radiance in the spectral interval 2190 to 2215 cm^{-1} and 2) - the temperature and water vapour profile retrieved at the first step.

For each given air mass type, the retrieved profiles were then compared to the test profiles to compute the root mean square error defined as:

$$e(p_i) = \left(\frac{1}{N_{obs}} \sum_{j=1}^{N_{obs}} (\hat{q}^{(j)}(p_i) - q^{(j)}(p_i))\right)^{\frac{1}{2}} \tag{8}$$

where $N_{obs} = 100$, $\hat{q}^{(j)}(p_i)$ is the retrieved concentration for the sample j at the i-th level pressure p_i, and $q^{(j)}(p_i)$ is the corresponding test value.

Figure 5 shows, for the various air mass types and for an N_2O perturbation of +5%, the vertical distribution of the root mean square error. It can be seen that in the lower and upper atmosphere the error almost coincides with the magnitude of the perturbation which means that there is no sensitivity to N_2O variations in the boundary layer and in the upper atmosphere. However, for pressures between 300 and 700 hPa the accuracy is of the order of 1% for the mid-latitude summer and tropical air masses, 1.5-2% for the mid-latitude winter and high-latitude summer air masses and around 3-4% for high-latitude winter air masses. We can thus conclude that with the exception of the high-latitude winter air masses the N_2O concentration profile between 300 and 700 hPa can be retrieved with a reasonable level of accuracy. The error analysis for the -5% perturbation case gives similar results as shown in Fig. 6.

In general, results show that for a perturbation of $\pm$ 5% the N_2O profile can be retrieved with a rms accuracy better than 2% for pressures between 300 and 700 hPa.

The sensitivity of the radiance to profile perturbation is shown in figure 7 where the Jacobian for a tropical air mass is plotted. It can be seen that the Jacobian peaks at pressures between 300 and 700 hPa and then attains

very low values for pressures either side of this range. Thus the low sensitivity to a perturbation in the boundary layer is intrinsic to the physical processes that govern the radiative transfer in the considered spectral range. However, it should be said that our analysis applies to the sea surface where the spectral emissivity is ≈ 1 or very close to 1 in the infrared. For surfaces characterised by a lower spectral emissivity, the performance of the retrieval scheme in the boundary layer is expected to improve.

To see how emissivity can influence the sensitivity of the retrieval in the boundary layer, let us consider the derivative of the spectral radiance with respect to the gas concentration q_1 in the lowest atmospheric layer (i.e. layer 1 in Table 1). If $R(\sigma)$ is the monochromatic spectral radiance, then by retaining only the leading terms of the derivative of the radiance with respect to q_1 (e.g., Amato et al (2002)), we can write

$$\frac{\partial R(\sigma)}{\partial q_1} = [-\varepsilon_o \tau_o B(T_g) + \tau_o B(T_1)] \frac{\partial \nu_1}{\partial q_1} \tag{9}$$

where ν_1 is the monochromatic layer optical depth for the considered gas specie, B is the Planck function, T_g and T_1 are the surface and the average layer temperature, respectively; τ_o is the total transmittance from the surface to the top of the atmosphere and finally ε_g is the spectral emissivity of the surface. For a sea surface we have typically $T_g \approx T_1$, so that if $\varepsilon_o \approx 1$, we have $\varepsilon_o \tau_o B(T_g) \approx \tau_o B(T_1)$ and the derivative is very close to zero: a change of concentration of N_2O at low altitudes is hard to be detected from space in the infrared.

Equation 9 applies to monochromatic radiance, therefore the sensitivity of the retrieval in the lower layers cannot be improved by increasing the spectral resolution of the sensor. This can only be achieved by making ε_o significantly lower than 1, i.e. the sensor has to look at low emissivity surfaces. Finally, it should be stressed that since Eq. 9 applies to any atmospheric gas, the accuracy of the retrieval in presence of highly emitting surfaces is going to be poor whatever the considered gas specie.

This said, Fig. 8 shows an example of retrieved N_2O profile for a tropical situation. The test profile is a climatological profile where the concentration of N_2O has been increased by 5% at all layers. As expected the retrieval just coincides with the first guess in the lower and upper atmosphere, and shows a good agreement with the test profile in between range 700 to 300 hPa.

For the same tropical situation, Fig. 9a shows the difference between the radiance spectra computed using the test and first guess atmospheric profiles (i.e. before the inversion). It can be seen that the first guess spectrum is biased to the test one. If we replace the first guess profile with the retrieved one, we can see in Fig. 9b that the bias is now greatly reduced with most of the points scattered randomly around zero.

The results and discussion above suggest that to check for changes in N_2O concentration we should choose the pressure range 300 to 700 hPa. In fact the better accuracy in terms of root mean square error (see Fig.s 5 and 6) is achieved at 550 hPa that is also where the N_2O Jacobian peaks.

For the numerical exercise described in this section, Tab. 2 compares the retrieved values at 550 hPa with the N_2O test concentration as a function of the air mass type. It can be seen that the concentration is retrieved almost unbiased with an accuracy which for the worst case is 3%. Table 2 applies to a perturbation of +5%, the -5% case gives the same results.

3.1.2 Quantifying retrieval interdependency

At the typical spectral sampling of 0.25 cm^{-1} (see Fig. 7) the N_2O Jacobian does not show any sharp feature. It is indeed very smooth and this poses severe limitations to the vertical spatial resolution of N_2O retrieval.

The resolving power or vertical spatial resolution of the spectral radiance is usually addressed in terms of the a-posteriori covariance matrix (e.g., Tarantola (1987)). For a given covariance matrix, the larger the off-diagonal

elements the worse the spatial resolution, since the parameters have not been independently retrieved from the data set, but only some linear combination of the parameters has been resolved.

To analyze the problem, we form the correlation matrix according to the usual definition:

$$\rho(i,j) = \frac{C(i,j)}{(C(i,i)C(j,j))^{\frac{1}{2}}} \tag{10}$$

where **C** is the a-posteriori retrieval covariance matrix (Eq. 5).

Figure 10b shows the correlation matrix for a typical retrieval example. We see that the dynamic range of the elements of the correlation matrix extends over the whole pressure range. This means that the correlation length scale does not tend to zero. Because of this behaviour, the inversion process can only resolve very smooth vertical structures such as those introduced by a systematic shift in the first guess solution. This perturbation has indeed a length scale $\rightarrow \infty$ and therefore compatible with the correlation structure of the retrieval.

The high correlation degree is a consequence of the intrinsic smooth nature of the Jacobian that makes the inverse problem severely ill-conditioned. Also the regularization parameter and the a-priori constraint which is here represented by the matrix **B** contribute to a less extent to the correlation of the final products. The matrix **B** has indeed a very short correlation length scale, as can be seen in Fig. 10a which shows the mesh surface of the **B**-correlation. We see that, in contrast to what happens in Fig. 10b, the elements of **B** drop rapidly to zero.

For the High-Latitude Winter atmosphere, Fig. 11 shows an histogram of γ_{opt} based on a sample of 100 retrievals. We see that γ_{opt} ranges mostly in between 0.2 to 2, which is a value at which regularization does contribute to the retrieval but does not dominate the final solution.

Finally, it should be stressed here that the vertical resolution could be improved by increasing the spectral resolution of the radiance.

3.2 Parametric approach to the estimation of N_2O concentrations

It has been shown in the previous section that the smooth structure of the N_2O Jacobian makes the inversion scantly sensitive to the shape of the profile. In the end, what we can hope to retrieve with a good level of confidence is a constant shift with respect to the reference profile.

Keeping this in mind, we can devise a faster and alternative retrieval algorithm provided that the relation between the observed and reference profile is:

$$q(p) = q_o(p)(1+a_s) \tag{11}$$

where a_s is a constant shift, $q(p)$ is the observed profile and $q_o(p)$ is the reference profile. If we assume the radiative transfer equation to be linear with respect to $q_o(p)$, we can write

$$R(i) = R_o(i) + \sum_{j=1}^{N_l} K(i,j)(q(j) - q_o(j)) = a_s \sum_{j=1}^{N_l} K(i,j) q_o(j) = a_s x(i) \tag{12}$$

where $x(i) = \sum_{j=1}^{N_l} K(i,j) q_o(j)$, K is the Jacobian matrix, $R(i)$ is the spectral radiance at wavenumber σ_i, $q(j)$ denotes the concentration at the j-th level pressure, and N_l is the number of atmospheric layers.

Using the same vector notation as in section 3.1, the above equation can be written as:

$$\delta\mathbf{r} = a_s\mathbf{x} \tag{13}$$

and the Least Square estimation $\hat{a}_s$ of a_s can be expressed as

$$\hat{a}_s = (\mathbf{x}'\mathbf{S}^{-1}\mathbf{x})^{-1}\mathbf{x}'\mathbf{S}^{-1}\delta\mathbf{r} \tag{14}$$

with the root mean square error $\delta\hat{a}_s$ given by:

$$\delta\hat{a}_s = \sqrt{(\mathbf{x}'\mathbf{S}^{-1}\mathbf{x})^{-1}} \tag{15}$$

The above estimation procedure has the advantage of being unbiased, for a perfect linear system, and does not require any kind of regularization.

For the same exercise shown in the previous section (i.e., $\pm$ 5% perturbation) the approach described here gives the results shown in Tab. 3. We can see that this approach gives fairly unbiased results, is able to retrieve the correct amount of shift even for the high-latitude winter atmosphere and is comparable, in terms of N_2O profile accuracy, to the non-parametric approach discussed in section 3.1.

4 Application to IMG spectra

In this section we consider for illustrative purposes examples of N_2O retrieval examples based on IMG observations. The set of IMG spectra we have used in our analysis is shown in Tab. 4. We have a total of five spectra, three of which have been recorded in the tropical belt (Indian Ocean and Atlantic Ocean) whereas the remaining two may be classified as mid-latitude winter spectra. Between the last two spectra one has been recorded over the Mediterranean sea and one over the Japan sea. The five observations are intentionally scattered across the globe to serve as a first check of the quality of the current N_2O climatology. In addition, the spectra are recorded over oceans and seas, that is in the natural, unpolluted atmosphere, where we expect N_2O to be uniformly mixed in the troposphere.

As discussed in section 2.3, the spectra have been convolved with a Gaussian function and re-sampled at the rate $\Delta\sigma = 0.25$ cm^{-1}. All the spectra are clear sky as shown by co-located Ocean Color and Temperature Scanner (OCTS) imagery.

The analysis at 550 hPa, based on the non-parametric approach described in section 3.1, gives the results shown in Tab. 5. It is possible to see that the retrieved quantities fluctuate by 2-5% around the corresponding climatological values, so that no evidence of any serious discrepancy between what is seen in the climatology and what is seen in the retrieval is revealed from the analysis of these data.

An example of non-parametric retrieval for the N_2O profile is shown in Fig. 12 which refers to the tropical IMG spectrum # 167229. As expected the retrieved profile coincides with the first guess in the lower and upper part of the atmosphere. Between 300 and 700 hPa, where we expect the highest sensitivity, the retrieval indicate an N_2O content that is slightly higher than the climatological value. The discrepancy with climatology is of the order of 4% and is statistically significant as shown by the error bars (see Fig. 12). All the analysed IMG spectra give a retrieved profile that always shows the same pattern: the retrieved profile is the first guess profile scaled by a scaling constant and the retrieval contains no new information about the shape of the observed N_2O profile.

This conclusion is further reinforced when we have a look at the difference between measured and simulated spectra. Figure 13 compares the radiance measured by IMG, the radiance simulated using the first guess profile and the difference between measured and first guess radiance. As in figures 8 and 9, the measured radiance is biased to the first guess radiance. When the measured radiance is compared to the one simulated using the retrieved profile (Fig. 14) the bias is greatly reduced and less than the IMG radiometric noise. However, if

we compare fig.14b with Fig. 9b we can now see that there are features not present before. Even though in principle these could be attributed to errors in the forward model they are more likely to be generated by a discrepancy between the real and assumed IMG instrumental response function.

Finally, for the case of the IMG spectrum # 167229, Fig. 15 compares the parametric to the non-parametric retrieval. The parametric approach estimates a shift of $+0.0396 \pm 0.0033$, which is perfectly in line with the one given by the non-parametric analysis. A look at the two retrieved profiles shown in Fig. 15 shows that exactly the same information is extracted by the two different approaches in the pressure range 300-700 hPa.

5 Conclusions

An inversion strategy to retrieve N_2O from radiance measured by high-resolution infrared sensors has been described. The strategy uses a sequential approach in which, first, temperature and water vapor are retrieved and then N_2O is inverted using the radiance measured in the range 2190-2215 cm^{-1}. Two different schemes have been developed and described. The first one is based on a physical scheme which is optimally regularized using the L-curve criterion (Hansen, 1992). The second one uses a simple parameterization of the observed profile in terms of a reference profile in which only the global amount of N_2O is changed whereas the vertical structure of the profile is left unchanged.

The performance of both methods has been evaluated in simulations using IASI-like spectra for different air mass types. Results show that the N_2O concentration can be retrieved with an accuracy of 1-3%. The sensitivity to the perturbation of N_2O profiles is maximum for pressures between 300 and 700 hPa. Both schemes requires the calculation of Jacobians. This is not a serious shortcoming since they can be pre-computed for a set of a reference profiles.

Based on the results discussed in the previous sections we can draw the following conclusions

- no information for N_2O can be obtained in the boundary layer by using spectra recorded over the sea surface,
- the amount of information that can be obtained regarding the shape of the observed N_2O profile is very limited,
- reliable information may be obtained for the N_2O total column amount
- the most appropriate pressure range to check whether or not a constant shift has occurred to the N_2O reference profile is 300 to 700 hPa.

The above first two items are not of serious concern since N_2O is uniformly mixed in the troposphere because of its long atmospheric residence time ($\approx$ 120 years).

Finally, examples of retrievals have been shown using IMG observations. Results confirm that both the non-parametric and parametric method give realistic results once applied to real observations. Although illustrative, the application to IMG spectra demonstrates that the concept of N_2O retrieval using spectra from infrared satellite-borne sensors does work.

Acknowledgment

Work supported by the Italian Space Agency. Marco Matricardi is supported by EUMESTSAT (contract EUM/CO/01/882/DK) through the IASI pre-launch definition studies.

References

Liou, K.N. 1992. *Radiation and Cloud Processes in the Atmosphere,*Oxford University Press, Oxford, UK, 487pp.

World Meteorological Organization (WMO) 2001. *WMO Global Atmosphere Watch World Data Centre for Greenhouse Gases,* CD-ROM no. 7, Published by Japan Meteorological Agency in cooperation with WMO.

Kobayashi, H., Shimota, A., Yoshigahara, C., Yoshida, I., Uehara, Y., Kondo, K. 1999. Satellite-borne high-resolution FTIR for lower atmosphere sounding and its evaluation, *IEEE Trans. Geosci. Remote Sensing,* vol. 37 (3), 1496-1507.

Amato, U., Masiello, G., Serio, C. and Viggiano, M. 2002. The σ-IASI code for the calculation of infrared atmospheric radiance and its derivatives, *Environmental Modelling & Software* Vol. 17/7, 651-667.

Clough, S.A., Iacono, M.J. and Moncet, J.-L. 1992. Line-by-line calculation of atmospheric fluxes and cooling rates, 1, Application to water vapor, *J. Geophys. Res.,* Vol. 97, 15,761-15,785.

Clough, S.A., Kneizys, F.X., Davies, R.W., 1989. Line shape and the water vapor continuum. *Atmospheric Research* **23**, 229-241.

Rothman, L.S., et al (1998). The HITRAN molecular spectroscopic database and HAWKS (Hitran Atmospheric Workstation): 1996 edition. Journal of Quantitative Spectroscopy and Radiative Transfer, Vol. 60, 665-710.

Lubrano, A.M., Serio C., Clough, S.A, Kobayashi, H. 2000. Simultaneous inversion for temperature and water vapor from IMG radiances, *Geophys. Res. Lett.,* Vol. 27, 2533-2536.

Amato, U., De Canditiis D., and Serio, C. 1998. Effect of apodization on the retrieval of geophysical parameters from Fourier-transform spectrometers, *Appl. Opt.* Vol. 37, No. 27, 6537-6543.

Masuda, K., Takashima, T., and Takayama, Y. 1988. Emissivity of pure and sea waters for the model sea surface in the infrared window regions, *Remote Sens. Environ.,* 24, 313-329.

Anderson, G.P., Clough, S.A., Kneizys, F.X., Chetwind, J.H., Shettle, E.P. 1986. *AFGL Atmospheric concentration profiles (0-120 km)* , AFGL-TR-86-0110, AFGL (OPI), Hanscom AFB, MA 01736.

Carfora, M. F., Esposito, F., and Serio, C. 1998. Numerical methods for retrieving aerosol size distribution from optical measurements of solar radiation, *J. Aerosol Sci.* Vol. 29, No. 10, 1225-1236.

Hansen, P.C. 1992. Analysis of discrete ill-posed problems by L-curve, *SIAM Rev.* Vol. 39, 561-580.

Kendall, M. and Stuart, A. 1979. *The advanced theory of statistics,* Vol. 2, 2nd Eidtion, C. Griffin, London, pp. 748.

Chedin, A., Scott, N.A., Wahiche, C. and Moulnier, P. 1985. The improved initiazilization inversion method: a high resolution method for temperature retrievals from satellites of the TIROS-N series, *Journal of Climate and Applied Meteorology,* **24**, 128-143.

Tarantola, A. 1987. *Inverse problem theory,* Elsevier Science B.V., London, UK, pp. 613.

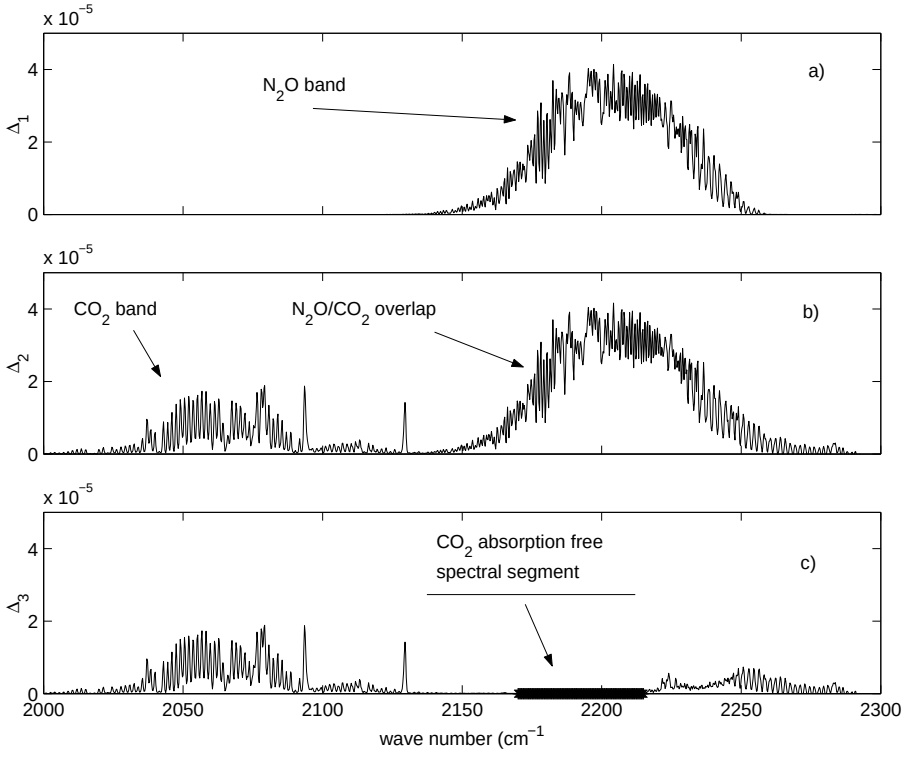

Figure 1: The difference between reference and test spectrum for a tropical air mass; a) the test spectrum is obtained perturbing the N_2O profile by +5%; b) the test spectrum is obtained perturbing simultaneously the N_2O and CO_2 profiles by +5% and +2% respectively. Figure 1c shows the difference $\Delta_3 = \Delta_1 - \Delta_2$ and evidences how the range 2170 to 2215 cm^{-1} is free from CO_2 absorption

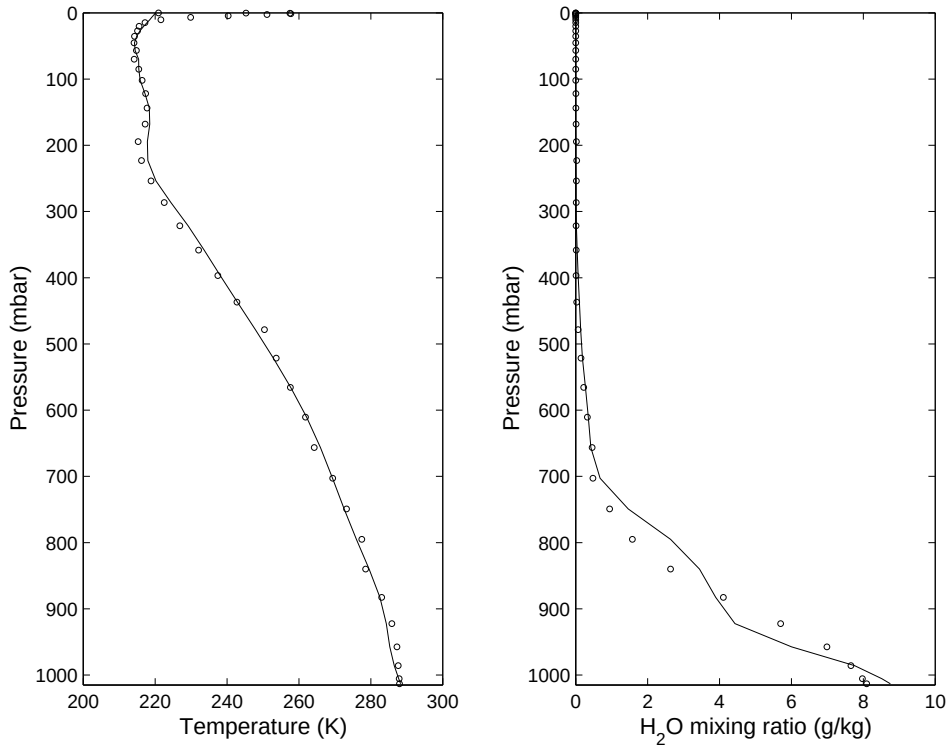

Figure 2: Example of temperature and water vapour profiles retrieved using the scheme discussed in (Lubrano et al, 2000). The inversion has been performed using the spectral ranges 667 to 830 cm^{-1} and 1100 to 1200 cm^{-1}. The retrieved profiles for the IMG mid-latitude winter spectrum # 327906, Obs.1 (see Table 4 for more details) are shown as circles in the figure. The ECMWF analysis for the same location and date is given as a solid line

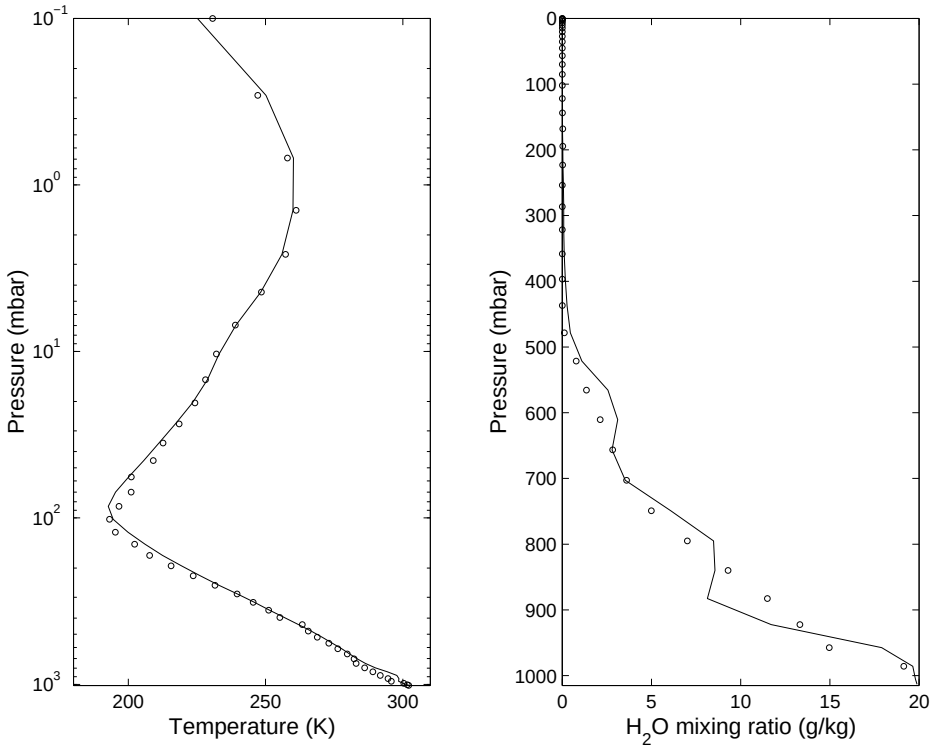

Figure 3: Example of retrieved temperature and water vapour profiles for the IMG tropical spectrum 374126, Obs. 2 (see Table 4 for mor e details). The retrieved profiles are shown as circles whereas the solid line denotes the ECMWF analysis for the same location and date. The profiles are plotted using a logarithmic scale to ease the comparison in the upper atmosphere.

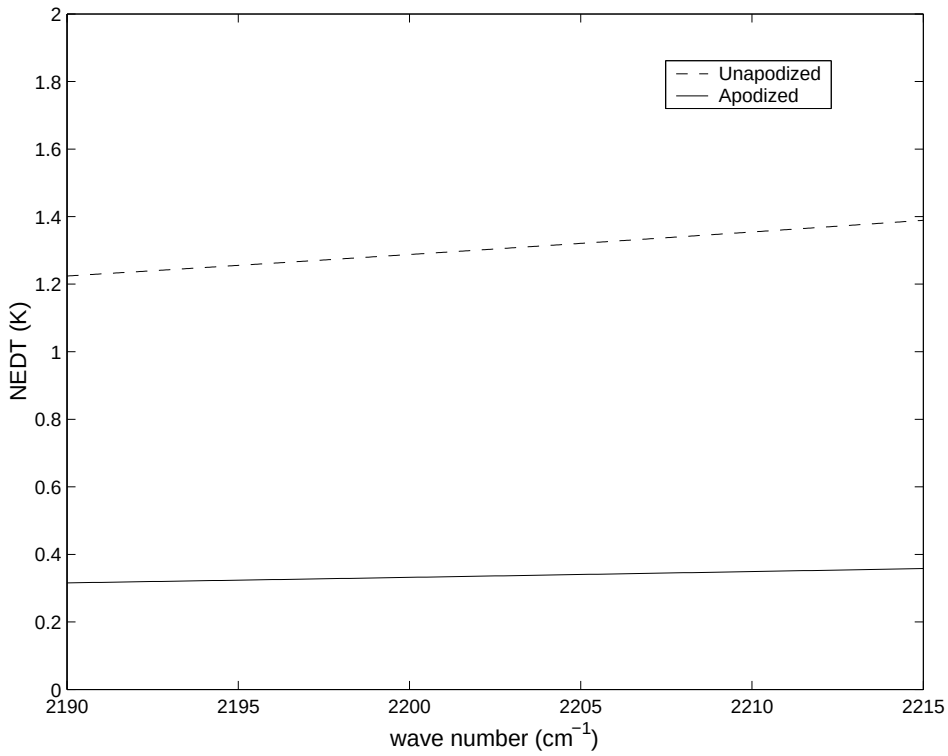

Figure 4: IMG radiometric noise expressed as NEDT for a scene temperature of 280 K. The dashed line is the radiometric noise at the le vel of unapodized radiance (sampling rate $\Delta\sigma = 0.05$ cm^{-1}; the solid line is the noise after apodization ($\Delta\sigma = 0.25$ cm^{-1}).

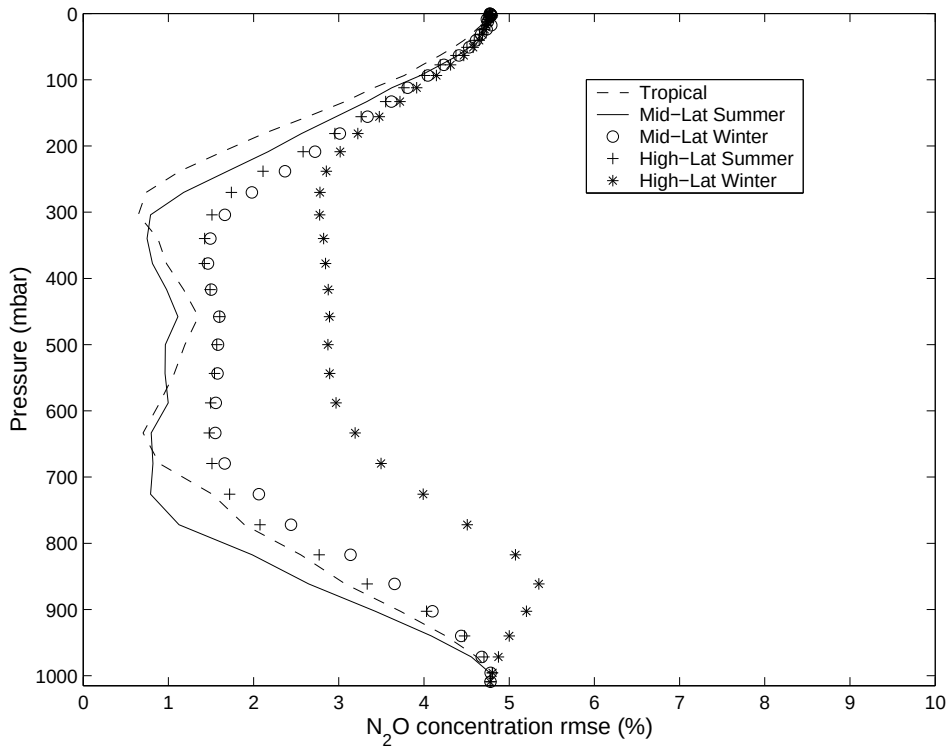

Figure 5: The accuracy of the retrieval scheme for a test case where the N_2O concentration profile is equal to 1.05 times its cli matological value (+5% perturbation). The figure shows the N_2O retrieval accuracy in terms of the root mean square error for the variou s air mass types.

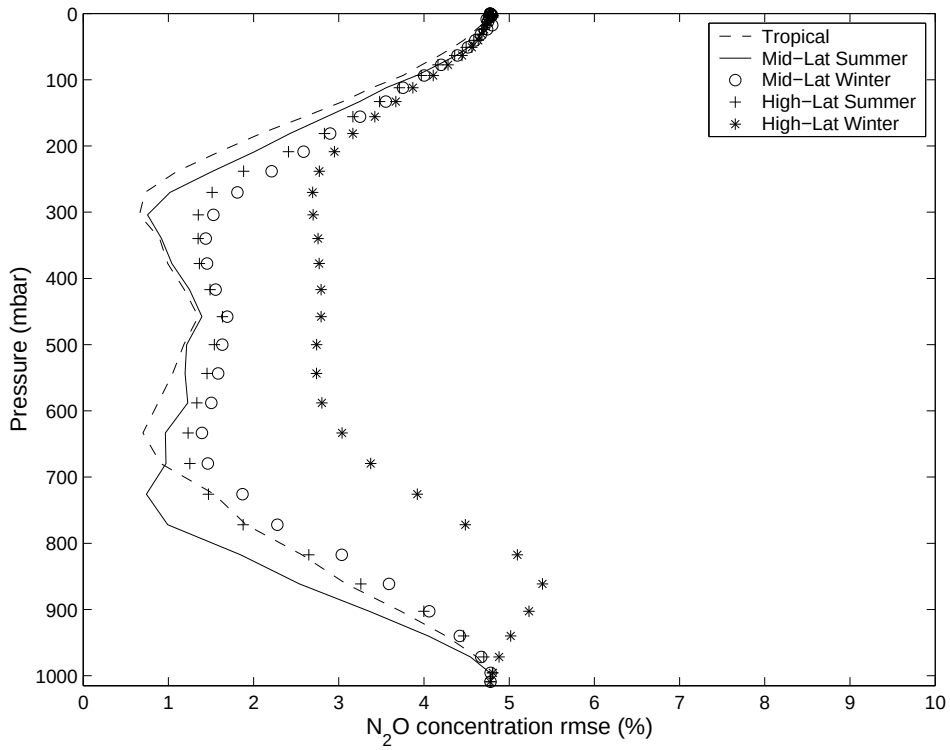

Figure 6: The accuracy of the retrieval scheme for a test case where the N_2O concentration profile is equal to 0.95 times its clima tological value (-5% perturbation). The figure shows the N_2O retrieval accuracy in terms of the root mean square error for the various air mass types.

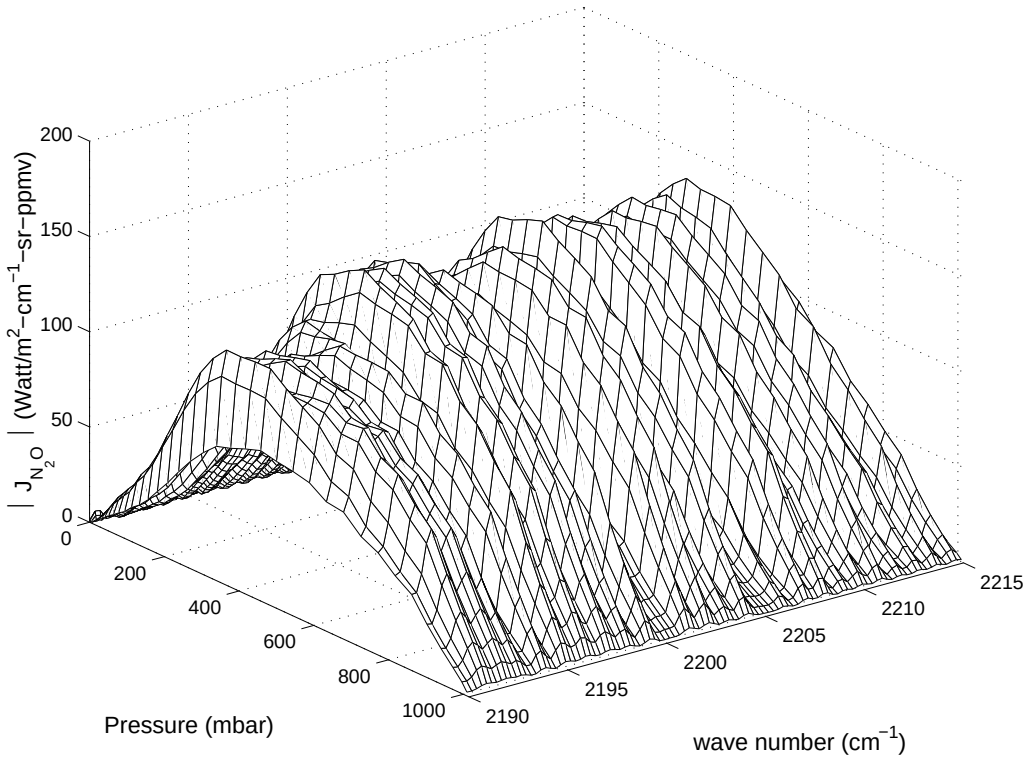

Figure 7: Absolute value of the N_2O Jacobian for a typical tropical air mass.

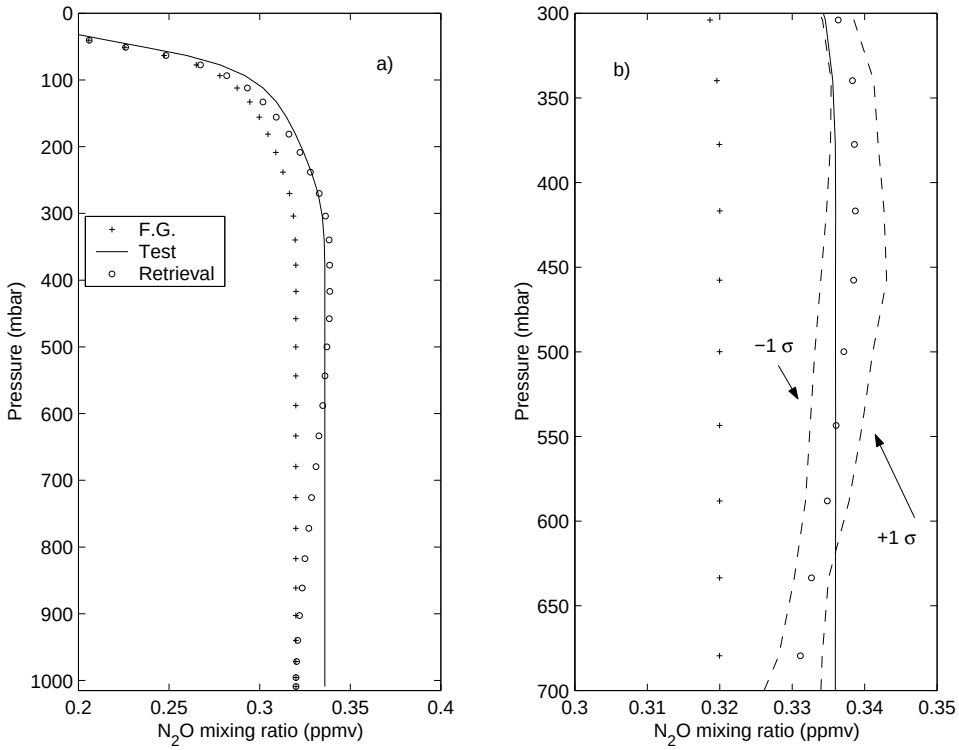

Figure 8: Example of retrieval for a tropical spectrum; a) - first guess, test and retrieved profiles are shown for the pressure range 0-1015 hPa; b) - as in a) but for the pressure range 300-700 hPa; the two dashed lines denote the $\pm$ *1* σ *tolerance interval.*

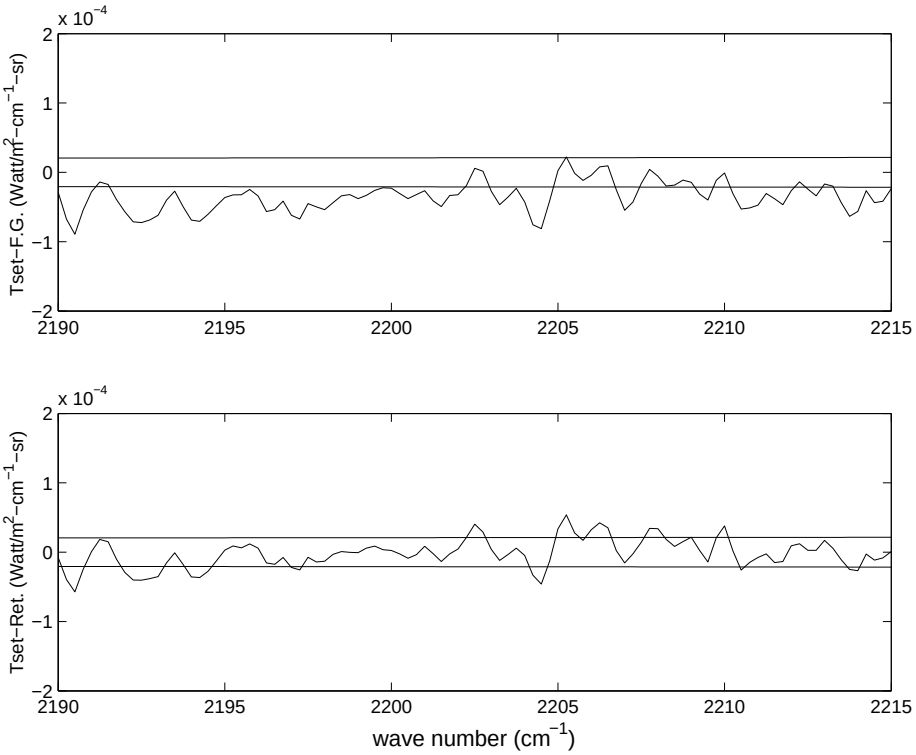

Figure 9: Spectral residual before (upper panel) and after the inversion (lower panel) for the retrieval example shown in Fig. 8. The t wo solid lines denote the $\pm 1\ \sigma$ tolerance interval (IMG radiometric noise).

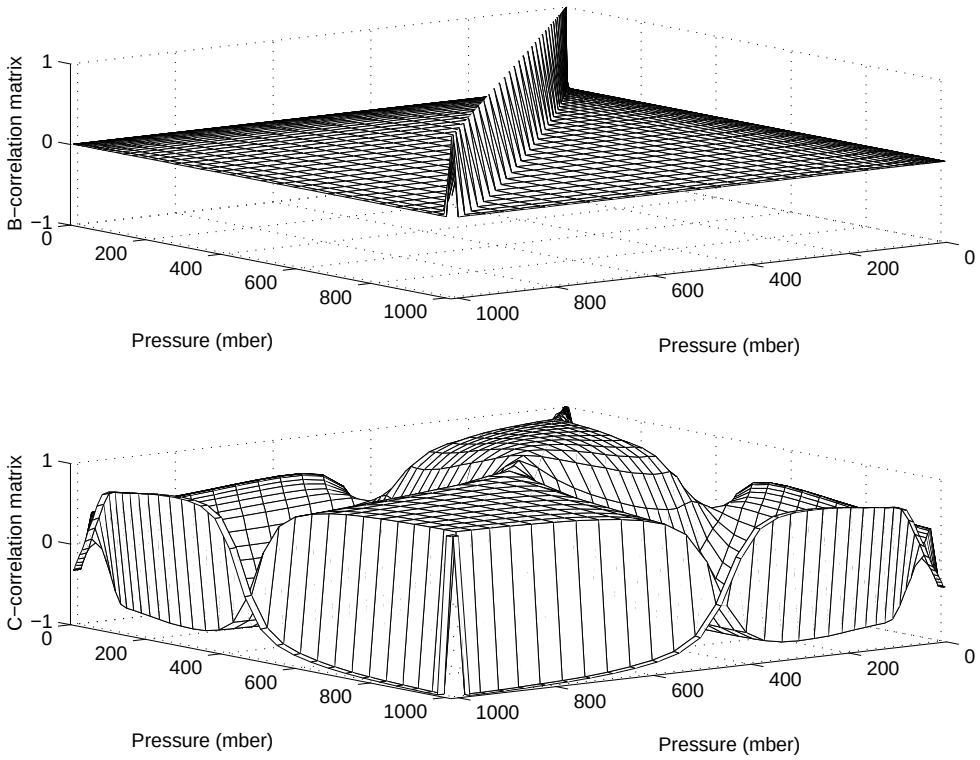

Figure 10: Correlation structure for **B** *matrix (upper panel) and the a-posteriori covariance matrix (lower panel).*

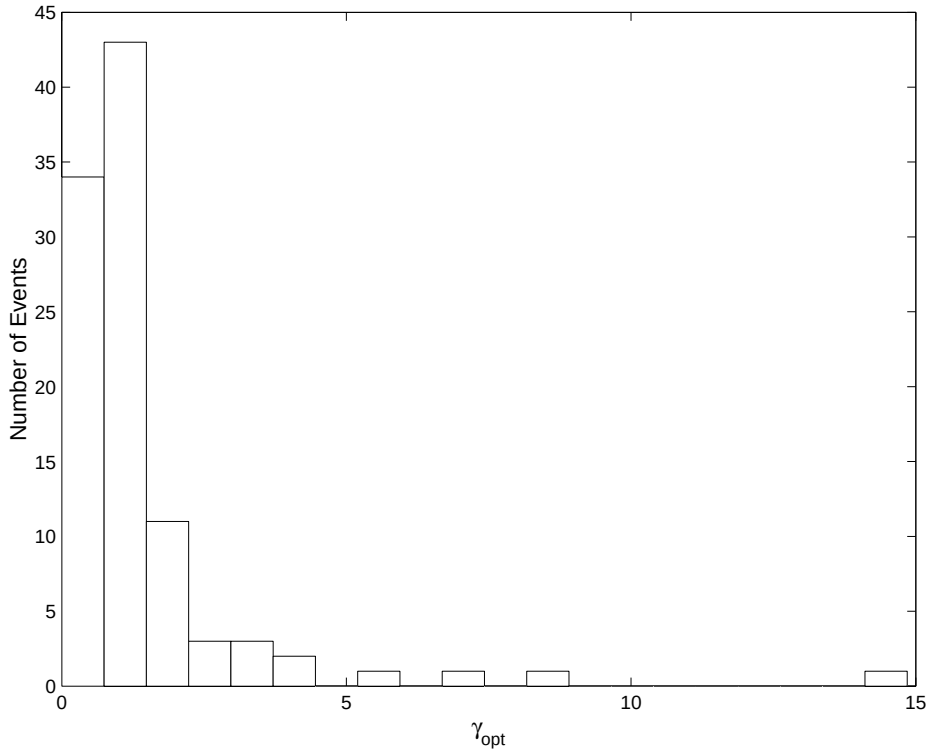

Figure 11: Histogram of γ_{opt} for the high-latitude winter 100-retrieval sample.

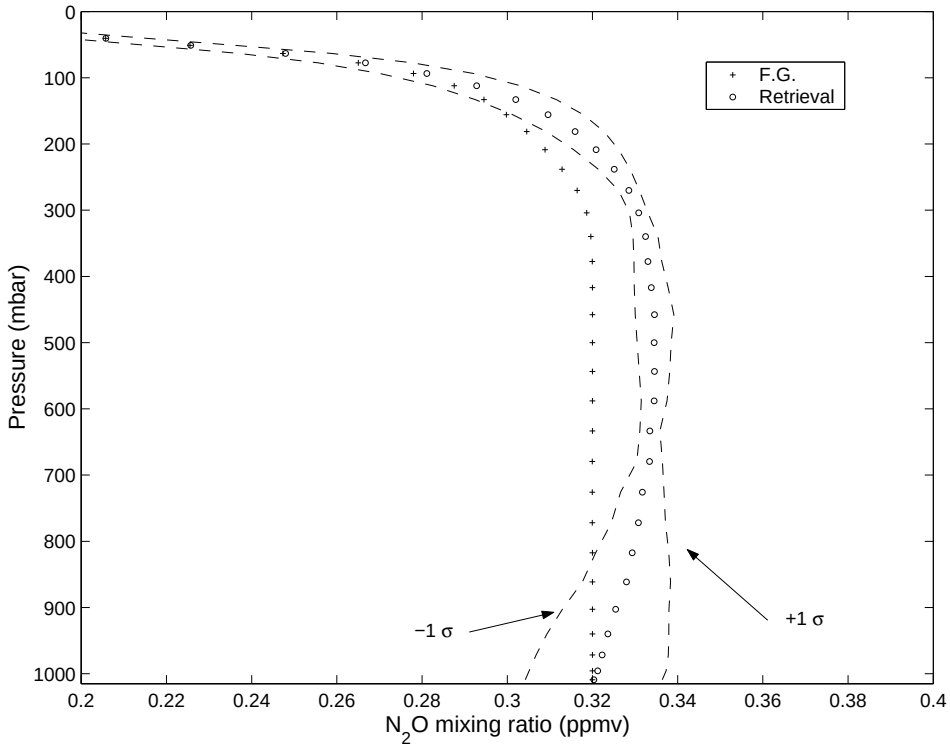

Figure 12: Example of non-parametric retrieval for a tropical IMG spectrum (# 167229). The ± 1 σ tolerance interval is sho wn as dashed line in the figure.

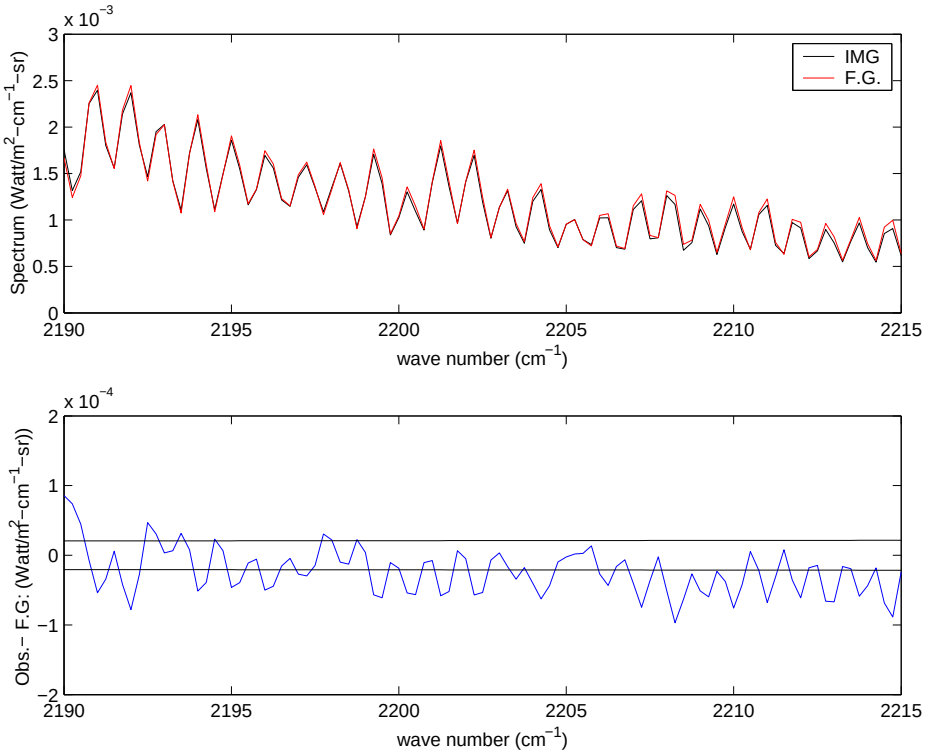

Figure 13: Observed and First Guess spectra (upper panel) for the retrieval example shown in Fig. 12. The difference between the two s pectra, spectral residual, is shown in the lower panel where the two solid lines denote the $\pm 1\,\sigma$ tolerance interval (IMG radiome tric noise).

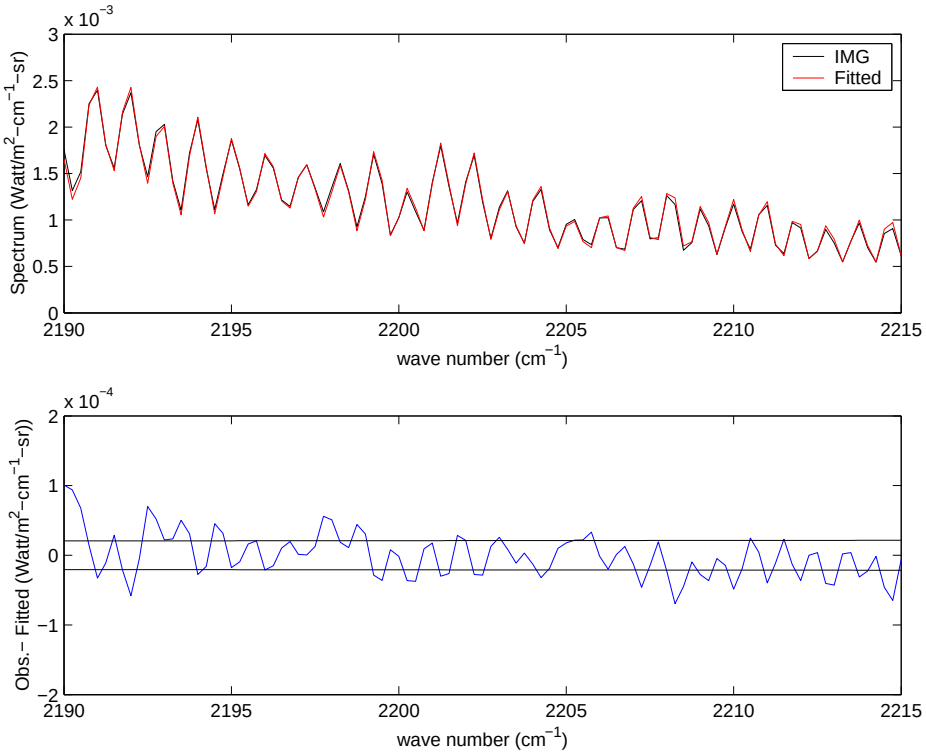

Figure 14: Observed and fitted spectra (upper panel) for the retrieval example shown in Fig. 12. The difference between the two spectr a, spectral residual, is shown in the lower panel where the two solid lines denote the $\pm 1\ \sigma$ tolerance interval (IMG radiometric noise).

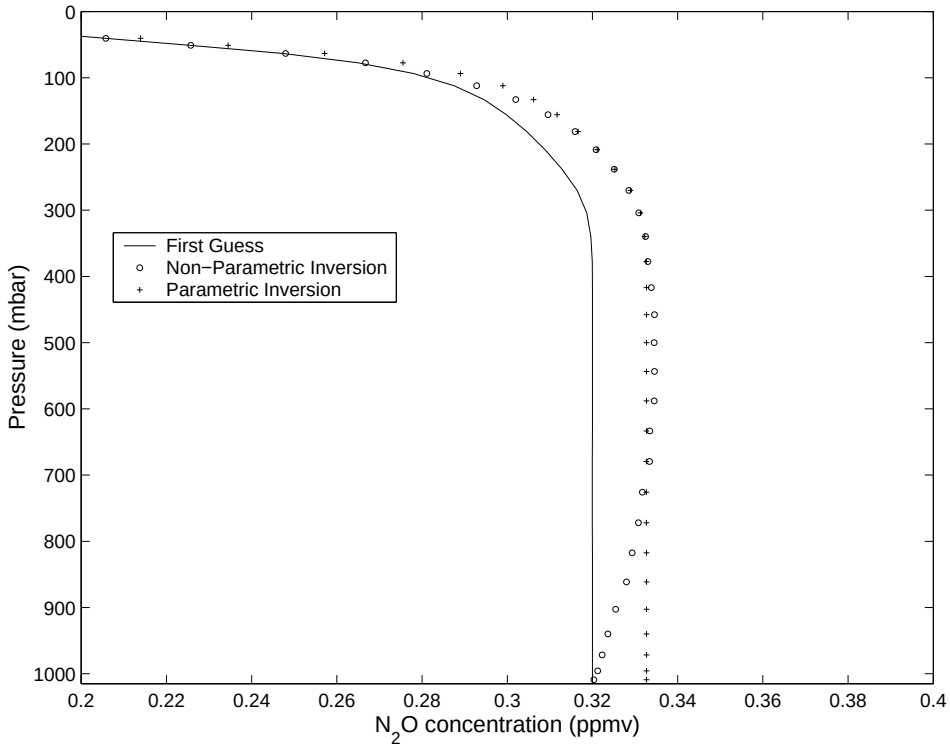

Figure 15: Comparison between the profiles retrieved using the parametric and non-parametric scheme for the tropical IMG spectrum # 1 67229.

Layer	Pressure (hPa)	Layer	Pressure (hPa)	Layer	Pressure (hPa)
1	1013.25 – 1005.43	16	436.95 – 396.81	31	45.29 – 35.51
2	1005.43 – 985.88	17	396.81 – 358.28	32	35.51 – 27.26
3	985.88 – 957.44	18	358.28 – 321.50	33	27.26 – 20.40
4	957.44 – 922.46	19	321.50 – 286.60	34	20.40 – 14.81
5	922.46 – 882.80	20	286.60 – 253.71	35	14.81 – 10.37
6	882.80 – 839.95	21	253.71 – 222.94	36	10.37 – 6.95
7	839.95 – 795.09	22	222.94 – 194.36	37	6.95 – 4.41
8	795.09 – 749.12	23	194.36 – 167.95	38	4.41 – 2.61
9	749.12 – 702.73	24	167.95 – 143.84	39	2.61 – 1.42
10	702.73 – 656.43	25	143.84 – 122.04	40	1.42 – 0.69
11	656.43 – 610.60	26	122.04 – 102.05	41	0.69 – 0.29
12	610.60 – 565.54	27	102.05 – 85.18	42	0.29 – 0.10
13	565.54 – 521.46	28	85.18 – 69.97	43	0.10 – 0.005
14	521.45 – 478.54	29	69.97 – 56.73		
15	478.54 – 436.95	30	56.73 – 45.29		

Table 1: Pressure layer grid used for forward and inverse calculations.

Air Mass Type	**First Guess** (ppmv)	**Test Value** (ppmv)	**Expec. Value** (ppmv)	**RMS Error** (ppmv)
Tropical	0.320	0.336	0.337	0.004
Mid-Latitude Summer	0.320	0.336	0.338	0.003
Mid-Latitude Winter	0.320	0.336	0.338	0.005
High Latitude Summer	0.299	0.315	0.316	0.005
High Latitude Winter	0.320	0.336	0.332	0.009

Table 2: Non-parametric estimation approach. Retrieval accuracy for N_2O concentration at 550 hPa in the case of a $+5\%$ perturbat ion of the first guess. The table shows the mean value and rms error of the retrieved concentration for a sample of 100 retrievals.

Air Mass Type	Test Value	Expectation Value	RMS error
Tropical	0.05	0.049	0.003
Mid-Latitude Summer	0.05	0.049	0.003
Mid-Latitude Winter	0.05	0.048	0.008
High Latitude Summer	0.05	0.050	0.008
High Latitude Winter	0.05	0.048	0.016

Table 3: Parametric approach. Retrieval accuracy for the case of a $+5\%$ shift. The table shows the mean value and rms error of the retrieved shift for a sample of 100 retrievals.

IMG record	Obs.	(Lat., Lon.) degrees	Date	GMT
374126	2	(11.92 N, 52.37 E)	6 May 1997	07:18
167229	1	(7.39 S, 50.63 E)	12 December 1996	07:14
167530	1	(12.14 S, 26.10 W)	12 December 1996	12:18
327906	1	(39.9 N, 8.9 E)	3 April 1997	21:36
166921	5	(39.61 N, 137.95 E)	12 December 1996	01:57

Table 4: IMG spectra used in the study.

IMG record	F.G. (ppmv)	Retrieved (ppmv)
374126	0.320	0.3099 ± 0.0036
167229	0.320	0.3346 ± 0.0036
167530	0.320	0.3202 ± 0.0036
327906	0.320	0.3078 ± 0.0053
166921	0.320	0.3242 ± 0.0053

Table 5: Non-parametric estimation approach. Estimated N_2O concentration at 550 hPa for the five IMG spectra listed in Tab. 4.